ChemComm

Accepted Manuscript

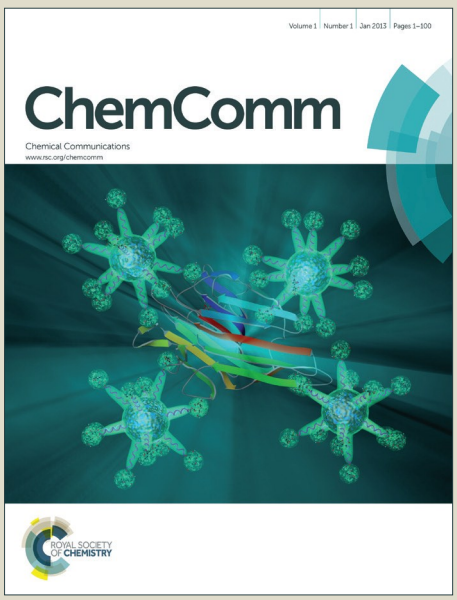

ROYAL SOCIETY OF CHEMISTRY

www.rsc.org/chemcomm

Journal Name

COMMUNICATION

A Quinary Layer Transition Metal Oxide of $NaNi_{1/4}Co_{1/4}Fe_{1/4}Mn_{1/8}Ti_{1/8}O_2$ as High Rate Capability and Long Cycle Life Cathode Material for Rechargeable Sodium Ion Batteries

Received 00th January 20xx,
Accepted 00th January 20xx

DOI: 10.1039/x0xx00000x

www.rsc.org/

Ji-Li Yue,[a] Wen-Wen Yin,[a] Min-Hui Cao,[a] Shadike Zulipiya,[a] Yong-Ning Zhou*[b] and Zheng-Wen Fu*[a]

A well-crystalized single phase quinary layer transition metal oxide of $NaNi_{1/4}Co_{1/4}Fe_{1/4}Mn_{1/8}Ti_{1/8}O_2$ was successfully synthesized. It exhibited excellent cycle performance and high rate capability as a cathode material for sodium-ion batteries.

Sodium-ion batteries have attracted more attentions for large-scale energy storage applications because of the natural abundance of sodium resources and low cost when compared to lithium and lithium ion batteries.[1-2] One of the most promising candidates of cathode materials for sodium ion batteriies is $NaMO_2$ (M= transition metals) layer-structured metal oxides due to their high capacity and ease of synthesis.[3-4] Unary metal oxide systems, $NaMO_2$ (M=Ti,[5] V,[6] Cr,[7] Mn,[8-9] Fe,[10] Co[11-12] and Ni[13-14]) have been extensively investigated as the cathodes for sodium ion batteries and each of them shows quite unique electrochemical performance. Environmental concerns are driving the research aiming to replace toxic metals such as Cr and V with harmfulless metals such as Ni, Co, Fe, Mn and Ti. The cooperative effect of various metals in layered metal oxides can often obtain unexpected electrochemical performance. Binary transition metal systems such as $NaNi_{1/2}Mn_{1/2}O_2$,[15] $NaFe_{1/2}Co_{1/2}O_2$,[16] $NaNi_{1/2}Ti_{1/2}O_2$[17] and $NaFe_{1/2}Mn_{1/2}O_2$[18] were put forward to increase the average voltage and the reversible capacity. Ternary systems, such as, $NaNi_{1/3}Co_{1/3}Mn_{1/3}O_2$,[19] $NaNi_{1/3}Co_{1/3}Fe_{1/3}O_2$,[20] $NaNi_{1/3}Fe_{1/3}Mn_{1/3}O_2$[21] and $Na(Ni_{1/2}Mn_{1/2})_xFe_{1-x}O_2$,[22-24] can smoothen the charge-discharge profile by preventing multiple transition or changes in the degree of distortion during the cycling. Quaternary systems, $NaNi_{0.25}Fe_{0.25}Co_{0.25}Mn_{0.25}O_2$[25] and $NaNi_{0.4}Fe_{0.2}Mn_{0.2}Ti_{0.2}O_2$[26] have been studied to further improve reversible capacity and selectively activate the reaction of desired elements. From previous studies,[27-29] it is known that doping the early transition metal in the layered compound may have some beneficial effects on the electrochemical behavior by changing its local electronic structure. It is very interesting to investigate the synergistic effects of each transition metal (Ni, Co, Fe, Mn and Ti) on the electronic and crystal structural changes and electrochemical performance in single layer-structured metal oxide compound. Here, we reported a single-phase quinary layer transition metal oxide of $NaNi_{1/4}Co_{1/4}Fe_{1/4}Mn_{1/8}Ti_{1/8}O_2$ (denoted hereafter as NCFMT) without any impurity for the first time (see Table S1). Its electrochemical performance as a new cathode material for SIBs is evaluated in a sodium half-cell. We reveal that this material has considerable reversible capacity, ultrafast charge-discharge capability and long cycle life for room temperature sodium-ion batteries.

Single phase NCFMT quinary solid solution is prepared by a simple solid state reaction. X-ray diffraction (XRD) pattern of the synthesized NCFMT is shown in Fig. 1a. All of the peaks can be well indexed to a hexagonal phase with a space group of R-3m. It is worth noting that there is no impure phase in the pristine NCFMT, which is quite different from the previously reported titanium-based electrode materials where the impure phases very often exist.[17, 30-32] The Rietveld refinement of the XRD pattern is carried out based on the structure of α-$NaFeO_2$. As shown in Table S2, the lattice parameters of NCFMT are a=b= 2.959 Å and c= 15.956 Å. The good agreement between the experimental pattern and the calculated one confirms the isostructure of NCFMT with α-$NaFeO_2$, which is built by repeating sheets of M-O_2 layer (M = Ni, Co, Fe, Ti and Mn) with Na ions being coordinated octahedrally by oxygen (Fig. 1b). Scanning electron microscopy (SEM) images of the synthesized NCFMT (Fig. 1c and d) show the size of the primary particles is about 1 ~ 2 μm. To futher clarify the microstructure of the sysnthesized NCFTM, high resolution transmission electron microscopy (HRTEM) was performed. HRTEM characterization suggests the two-dimension fringes have the same d-spacing of 0.257 nm, which can be attributed to the (010) and (100) planes (Fig. 1e),

[a] Shanghai Key Laboratory of Molecular Catalysts and Innovative Materials, Department of Chemistry & Laser Chemistry Institute, Fudan University, Shanghai, 200433, P.R. China. E-mail: zwfu@fudan.edu.cn
[b] Department of Materials Science, Fudan University, Shanghai, 200433, P.R. China. E-mail: ynzhou@fudan.edu.cn

† Footnotes relating to the title and/or authors should appear here.
Electronic Supplementary Information (ESI) available: [details of any supplementary information available should be included here]. See DOI: 10.1039/x0xx00000x

and the Fast Fourier Transform (FFT) corresponding to the fringes is also displayed in the insets. In order to confirm the element constituents of this material, energy dispersive spectroscopy (EDS) was conducted and shown in Fig. 1f. The obvious spectrum peaks confirm the existence of sodium, titanium, manganese, iron, cobalt, nickel and oxygen elements in the samples (Fig. 1f and Table S3). The valance states of the transition metals in NCFMT were invesgated by K-edge X-ray absorption near edge structure (XANES) spectroscopy (Fig. S1). By comparing the edge positions in XANES, we can estimate that the valence states of the Ni, Co, Fe, Mn and Ti ions in the pristine NCFMT are 2+, 3+, 3+, 4+ and 4+, respectively.

The galvanostatic charge-discharge curves of the NCFMT electrode cycled between 2.0-4.1 V vs. Na^+/Na at a current density of 13 mA g^{-1} are shown in Fig. 2a. The open circuit voltage (OCV) lies close to 2.7 V. In the initial charge process, a flat voltage plateau from 2.7 to 3.1 V is followed by a sloping voltage plateau from 3.1 to 4.1 V. The initial charge capacity is found to be 131 mAh g^{-1}, which corresponds to about 0.54 Na deintercalated per NCFMT. In the initial discharge process, a quite symmetric curve comparing with the charge process is observed. It includes a sloping region from 4.1 V to 2.8 V followed by a flat plateau at around 2.7 V. The initial discharge process yield a specific capacity of 128 mAh g^{-1}, which is about 98% of the initial charge capacity, indicating a quite high coulombic efficiency during the first cycle. In the subsequent cycles, the discharge curves are almost overlapped with the initial one, demonstrating an excellent reversibility.

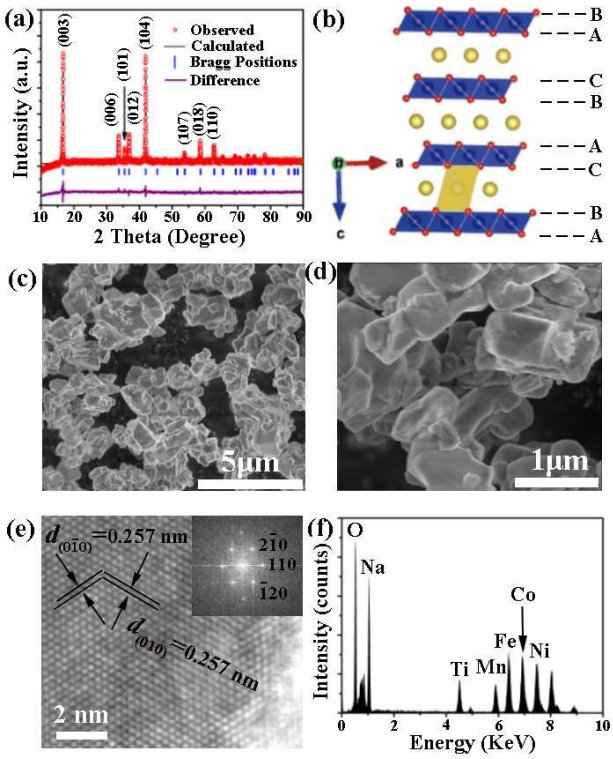

Fig. 1 (a) X-ray diffraction pattern and Rietveld refinement of the as-prepared NCFMT sample. (b) Schematic of the O3-NCFMT crystal structure, legend: red, blue and yellow balls stand for oxygen, transition metal and sodium ions, respectively. (c) Low and (d) high magnification SEM images of the O3-NCFMT material. (e) TEM image and corresponding FFT (inset). (f) EDX analysis results.

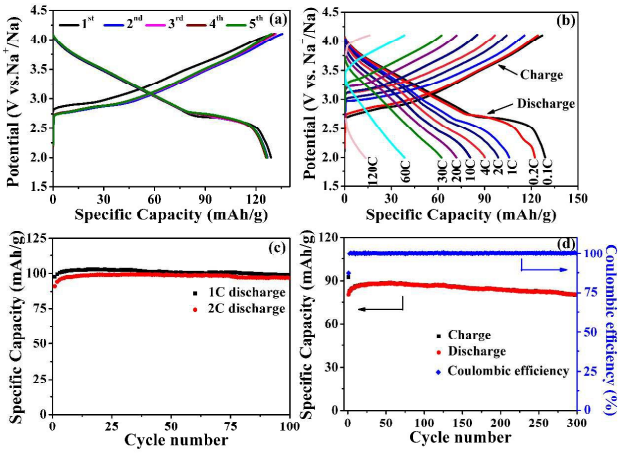

Fig. 2 (a) The galvanostatic charge/discharge curves of NCFMT in the initial five cycles at a current rate of 0.1C (13 mA g^{-1}) in the potential range of 2.0 – 4.1V versus Na^+/Na, (b) Rate capability at various current densities, (c) Cyclic performances of the NCFMT electrode cycled at a current density of 1C and 2C. (d) Long term cyclic performances and coulombic efficiencies of the NCFMT electrode cycled at a current density 4C.

The typical discharge curves of NCFMT at different C rate (1C rate is calculated based on a specific capacity of 130 mAh g^{-1}) are shown in Fig. 2b. A specific capacity of 128.89, 122.33, 105.81, 98.72, 90.13, 80.7, 71.8 and 62.3 mAh g^{-1} were obtained at the current densities of 0.1 C, 0.2C, 1C, 2C, 4C, 10C, 20C and 30C respectively. Even at 60 and 120C, the material still can deliver a discharge capacity of 38.6 and 13.6 mAh g^{-1}. The high rate capacity was tentatively ascribed to a synergy effects on an increase in the inter-slab spacing leading to improved sodium diffusion by titanium substitution[33] and improved the charge carrier transport properties by manganese addition.[34] Further investigation in detail is under progress to study the interplay of all the transition metal substitution. The cycle performance of this material at 1C and 2C rate shown in Fig. 2c indicates that there is an activation process during the initial cycles. The reversible capacities progressively increase during the first few cycles and ultimately reaches maximum values of 102.82 and 99.07 mA h g^{-1} at 1C and 2C, respectively. NCFMT electrode remain reversible capacities of 98.83 and 96.82 mAh g^{-1} after 100 cycles, corresponding to a capacity retention of 96.12% and 97.72%, respectively. Fig. 2d shows the long-term cyclic performance at a rate of 4C. It can be seen that the behavior is similar with 1C and 2C, a maximum capacity of 88 mAh g^{-1} was obtained in the 27th cycle and 90.68% of the maximum specific capacity is maintained after 300 cycles at 4C with a capacity-decay rate about 0.035% per cycle, indicating a

superior long-term cyclic ability, and the average coulombic efficiency was close to 100%. Such good cycling properties imply that NCFMT might be a very attractive cathode material for rechargeable Na-ion batteries. The electrochemical properties of various layered cathode materials are listed to confirm the novelty of the NCFMT cathodes developed in the present work (Table S1). This comparison demonstrates the competitiveness of the NCFMT material in terms of capacity retention during prolonged cycling and such high rate (4C) capability, which have not been achieved previously in layer transition metal oxide for rechargeable Na battery systems. NCFMT electrode can deliver a capacity of 142 mAh g^{-1} if the electrode is charged to 4.2V, but the capacity drops to 105 mAh g^{-1} after ten cycles, corresponding to an average capacity fading rate of 3% per cycle (Fig S2).

To understand the structure evolution of the NCFMT during Na^+ deintercalation from the NCFMT host, XRD patterns were collected at different charge states during the first charge process, as shown in Fig. 3. The (003) and (006) peaks reflect the change of lattice parameter *c*, while (101) and (012) peaks mainly reflect the change of lattice parameter *a* and *b*. At the beginning of the charge, a new (003) peak emerges at lower two-theta angles. As is known to all, the (003) peak is a single-fold peak. Thus, every new (003) peak is a fingerprint for the formation of a new phase. Combining with other diffraction peaks, the new formed phase is resolved as a P3 stacking ordering. In the range of $0<x<0.125$, two-phase coexistence could be observed. The intensity of the (003) peak for the second phase increases with increasing Na-ion extraction in expense of that for the first one, indicating a two-phase reaction. In the range of $0.125<x<0.54$, the (003) peak of the pristine O3 phase disappears, and the (003) peak of the new formed P3 phase dominates. The new (003) peak keeps shifting to lower two-theta angles, suggesting a solid-solution reaction in this region. In the whole charge process, the (003) and (006) shift to the lower angles, while (101) and (102) shift to the high angles, indicating that lattice parameter *c* increases while *a*(*b*) decreases during charge. This

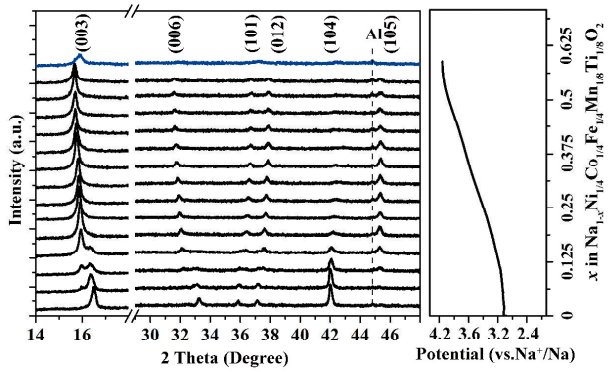

Fig. 3 Structure evolution of NCFMT during the first charge. *Ex* situ X-ray diffraction patterns collected during the first charge of the Na/ NCFMT cells under a current rate of 10 mA g^{-1} up to 4.1V. The corresponding voltage–composition profile is given on the right side of XRD patterns.

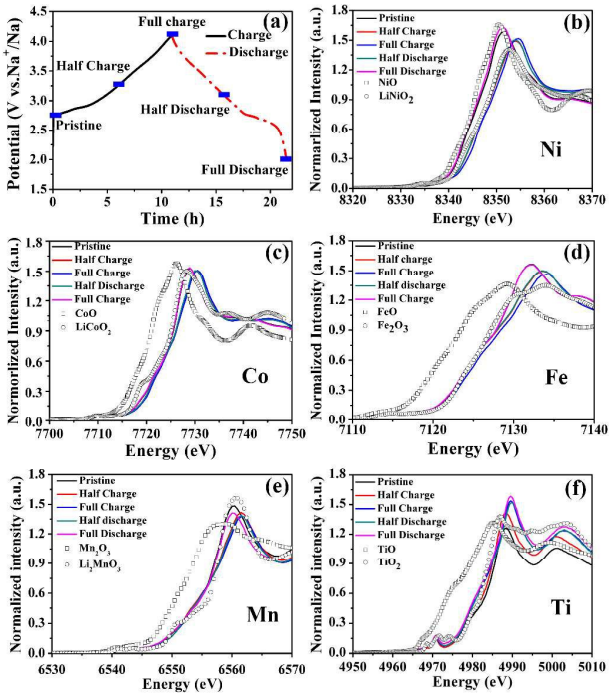

Fig. 4 (a) Charge and discharge curve of NCFMT electrode for ex XAFS, blue solid squares on the curve stand for the state where XAS data were obtained. (b), (c), (d), (e) and (f) Normalized XANES of NCFMT at various charge and discharge stages during the first cycle at Ni, Co, Fe, Mn and Ti K-edges, respectively.

is a typical unit cell breathing behavior of the layer-structured cathode materials in the charge process. If the Na-ions are extracted further (when $x>0.54$), the (003) peak will shift to higher 2ϑ angle (blue line), indicating the collapse of the layered structure along *c* axis. This irreversible structure change will result in severe capacity fading (Fig. S2). While there is a significant reduction of capacity fading by limiting the potential range of 2.0-4.1V (Fig. 2). To further investigate the local structure and valence state changes of Ni, Co, Fe, Mn and Ti of the NCFMT duringcharge and discharge, *ex* situ X-ray absorption spectroscopy at the Ni, Co, Fe, Mn and Ti K-edge were carried out. The blue solid squares on the curve in Fig. 4a stand for the state where XAS data were obtained. Fig. 4 b, c, d, e and f show the Ni, Co, Fe, Mn and Ti K-edge X-ray absorption near edge structure (XANES) spectra during the first charge and discharge process, respectively. For the Ni K-edge (Fig. 4b), a rigid shift of the edge to high energy is observed, indicating the oxidation of Ni^{2+} during Na ions extraction. The absorption edge at the half charged state (about 3.4 V) is quite similar to the reference compound $LiNiO_2$, indicating the valance state of Ni in NCFMT is changing from 2+ to 3+ during the low potential region (OCV - 3.4 V), the absorption edge at the fully charged state is slightly higher than the reference compound $LiNiO_2$, implying Ni^{3+} ions are further oxidized. During the discharge process, the edge position finally recovers its pristine state, suggesting Ni was

reduced back to Ni^{2+} after discharge. For Co and Fe (Fig. 7c and d), the absorption edge nearly unchanged before half charge, small shifts of the edge position to higher energy are observed after half charge. Compared with the XANES spectrum of metal oxide references, it can be estimated that the valence states of Co and Fe after fully charge are between 3+ and 4+. Upon discharge,the XANES spectrum of Co and Fe undergo opposite evolutions comparing to the charge process, and finally recover their pristine states, suggesting the reversible change of the electronic structure and surrounding environment of Co and Fe in NCFMT. For Mn and Ti (Fig. 4e and f), the energy positions of K-edges do not shift, but with little shape changes during the charge and discharge process. It is reasonable because the valance state of Mn and Ti are 4+ in the pristine NCFMT. It is very hard to oxidize Mn^{4+} and Ti^{4+} to a higher valence state by electrochemical charge. The little changes of the edge shapes indicate some local environment changes around Mn and Ti ions during the charge and discharge process. During the Na^+ deintercalation/intercalation processes, Ni, Co and Fe contribute to the charge compensation, while Mn and Ti stabilize the structure without changed their oxidation states.

In summary, a quinary layer-structured metal oxide of $NaNi_{1/4}Co_{1/4}Fe_{1/4}Mn_{1/8}Ti_{1/8}O_2$ compound was successfully synthesized and studied as a cathode material for sodium ion batteries. Combining its high rate capability and long cycle life, NCFMT could be a very promising cathode material for room temperature high power sodium-ion batteries. On the other hand, a pure layer compound NCFMT containing five metal elements provides a good example for studying some fundamental science issues in layer oxide, such as the effect of each transition metal ions in the layer-structured cathode system and their synergistic effect.

This work was financially supported by the NSAF (Grant No.U1430104), and National Foundation of China (no. B1120132029). The authors thank Beamline BL14W1 of the Shanghai Synchrotron Radiation Facility in China for providing the beam time.

Notes and references

1 N. Yabuuchi, K. Kubota, M. Dahbi and S. Komaba, *Chem. Rev.*, 2014, **114**, 11636-11682.
2 D. Kundu, E. Talaie, V. Duffort and L. F. Nazar. *Angew. Chem. Int. Ed.*, 2015, **54**, 3431-3448.
3 K. Kubotu, N. Yabuuchi, H. Yoshida, M. Dahbi and S. Komaba, *MRS Bull.*, 2014, **39**, 416-422.
4 M. H. Han, E. Conzalo, G. Singh and T. Rojo, *Energy Environ. Sci.*, 2015, **8**, 81–102.
5 D. Wu, X. Li, B. Xu, N. Twu, L. Liu and G. Ceder. *Energy Environ. Sci.*, 2015, **8**, 195-202.
6 D. Hamani, M. Ati, J. M. Tarascon and P. Rozier, *Electrochem. Commun.*, 2011, **13**, 938–941.
7 S. Komaba, C. Takei, T. Nakayama, A.Ogata and N. Yabuuchi, *Electrochem. Commun.*, 2012, **12**, 355–358.
8 X. H. Ma, H. L. Chen and G. Ceder, *J. Electrochem. Soc.*, 2011, **158**, A1307-A1312.
9 J. Billaud, R. J. Clement, A. R. Armstrong, J. Canales-Vazquez, P. Rozier, C. P. Grey and P. G. Bruce, *J. Am. Chem. Soc.*, 2014, **136**, 17243−17248.
10 N. Yabuuchi, H. Yoshida and S. Komaba, *Electrochemistry*, 2012, **80**, 716-719.
11 J. J. Ding, Y. N. Zhou, Q. Sun, X. Q. Yu, X. Q. Yang and Z. W. Fu, *Electrochimica Acta*, 2013, **87**, 388-393.
12 T. Shibata, Y. Fukuzumi, W. Kobayashi and Yutaka Moritomo, *Sci. Rep.*, 2015, **5**, 9006.
13 P. Vassilaras, X. H Ma, X. Li and G. Ceder, *J. Electrochem. Soc.*, 2013, **160**, A207-A211.
14 M. H. Han, E. Gonzalo, M. Casas-Cabanas and T. Rojo, *J. Power Sources*, 2014, **258**, 266-271.
15 S. Komaba, N. Yabuuchi, T Nakayama, A. Ogata, T. Ishikawa and I. Nakai, *Inorg. Chem.*, 2012, **51**, 6211−6220.
16 H. Yoshida, N. Yabuuchi and S. Komaba, *Electrochem. Commun.*, 2013, **34**, 60-63.
17 H. J. Yu, S. H. Guo, Y. B. Zhu, M. Ishida and H. S. Zhou, *Chem. Commun.*, 2014, **50**, 457-459.
18 N. Yabuuchi, M. Kajiyama, J. Iwatat, H. Nishikawa, S. Hitomi, R. Okuyama, R. Usui, Y. Yamada and S. Komaba, *Nat. Mater.*, 2012, **11**, 512-517.
19 M. Sathiya, K. Hemalatha, K. Ramesha, J.-M. Tarascon and A. S. Prakash, *Chem. Mater.*, 2012, **24**, 1846−1853.
20 P. Vassilaras, A. J. Toumar and G. Ceder, *Electrochem. Commun.*, 2014, **38**, 79–81.
21 D. Kim, E. Lee, M. Slater, W. Lu, S. Rood and C.S. Johnson, *Electrochem. Commun.*, 2012, **18**, 66–69.
22 N. Yabuuchi, M. Yano, H. Yoshida, S. Kuze and S. Komaba, *J. Electrochem. Soc.*, 2013, **160**, A3131−A3137.
23 S. M. Oh, S. T. Myung, C. S. Yoon, J. Lu, J. Hassoun, B. Scrosati, K. Amine and Y.K. Sun, *Nano Lett.*, 2014, **4**, 1620.
24 D. D. Yuan, Y. X. Wang, Y. L. Cao, X. P. Ai and H. X. Yang, *ACS Appl. Mater. Interfaces*, 2015, **7**, 8585−8591.
25 X. Li, D. Wu, Y. N. Zhou, L. Liu, X. Q. Yang and G. Ceder, *Electrochem. Commun.*, 2014, **49**, 51-54.
26 X. Sun, Y. Jin, C. Y. Zhang, J. W. Wen, Y. Shao, Y. Zang and C. H. Chen, *J. Mater. Chem. A*, 2014, **2**, 17268–17271.
27 Y. N. Zhou, J. Ma, E. Y. Hu, X. Q. Yu, L. Gu, K. W. Nam, L. Q. Chen, Z. X. Wang and X. Q. Yang, *Nat. Commun.*, 2014, **5**, 5381.
28 J. Ma, Y. N. Zhou, Y. R. Gao, Q. Y. Kong, Z. X. Wang, X. Q. Yang and L. Q. Chen, *Chem. Eur. J.*, 2014, **20**, 8723–8730.
29 I. M. Markus, F. Lin, K. C. Kam, M. Asta and M. M. Doeff, *J. Phys. Chem. Lett.*, 2014, **5**, 3649-3655.
30 Y. S. Wang, J. Liu, B. Lee, R. M. Qiao, Z. Z. Yang, S. Y. Xu, X. Q. Xu, L. Gu, Y. S. Hu, W. L. Yang, K. Kang, H. Li, X. Q. Yang, L. Q. Chen and X. J. Huang, *Nat. Commun.*, 2015, **6**, 6401.
31 J. Wang, B. Qiu, X. He, T. Risthaus, H. Liu, M. Cristian Stan, S. Schulze, Y. Xia, Z. Liu, M. Winter and J. Li, *Chem. Mater.*, 2015, **27**, 4374−4379.
32 G. Singh, F. Aguesse, L. Otaegui, E. Goikolea, E. Gonzalo, J Segalini and T. Rojo. *J. Power Sources*, 2015, **273**, 333-339.
33 K. C. Kam, A. Mehta, J. T. Heron and M. M. Doeff, *J. Electrochem. Soc.*, 2012, **159**, A1383−A1392.
34 R. Shanmugam and W. Lai, *J. Electrochem. Soc.*, 2015, **162**, A8−A14.